https://doi.org/10.5194/acp-2022-360
Preprint. Discussion started: 14 June 2022


Atmospheric Chemistry and Physics
Discussions

# Quantitative impacts of vertical transport on long-term trend of nocturnal ozone increase over the Pearl River Delta region during 2006-2019

Yongkang Wu[1,2], Weihua Chen[1,2,*], Yingchang You[1,2], Qianqian Xie[1,2], Shiguo Jia[3], Xuemei Wang[1,2]

[1]Institute for Environmental and Climate Research, Jinan University, Guangzhou, 510632, P. R. China
[2]Guangdong-Hongkong-Macau Joint Laboratory of Collaborative Innovation for Environmental Quality, Guangzhou 511443, China
[3]School of Atmospheric Sciences, Sun Yat-sen University and Southern Marine Science and Engineering Guangdong Laboratory (Zhuhai), Zhuhai, 519082, China

*Correspondence:* Weihua Chen (chenwh26@163.com)

**Abstract.** The Pearl River Delta (PRD) region in southern China has been facing severe ozone ($O_3$) pollution during the day, as well as anomalous nocturnal $O_3$ increase (NOI) during the night. In this study, relying on observed surface and vertical $O_3$ and the fifth-generation European Centre for Medium-Range Weather Forecasts (ECMWF) reanalysis (ERA5) dataset, the spatiotemporal variation of NOI events is comprehensively analysed and the role of vertical transport in the occurrence of NOI events is quantified in the PRD region from 2006 to 2019. Results show that the annual average frequency of NOI events is estimated to be 53 ± 16 d $yr^{-1}$ in the PRD region during the 14-year period, with 58 ± 11 μg $m^{-3}$ for the nocturnal $O_3$ peak (NOP) concentration on average. Low-level jets (LLJs) and convective storms (Conv) are the main meteorological processes that induce NOI events, explaining 61 % and 11 % of NOI events on average, respectively. Annually, NOI events exhibit an upward trend (4.70 d $yr^{-1}$) before 2011 and a downward trend (-0.72 d $yr^{-1}$) afterward, which is consistent with the annual variation of LLJs ($r=0.88$, $p<0.01$). Although the contribution of Conv to NOI events is relatively small, Conv-induced NOI events continuously increase at a rate of 0.26 d $yr^{-1}$ during this 14-year period owing to the effect of expanding urbanization. Seasonally, relatively higher frequency of NOI events is observed in spring and autumn, which is consistent with the seasonal pattern of LLJs and maximum daily average 8-h (MDA8) $O_3$. Spatially, NOI events are frequent in the eastern PRD, which matches well with the spatial distribution of LLJ frequency while partially overlapping with the distribution of MDA8 $O_3$ concentration, suggesting a more important role for vertical transport than for daytime $O_3$ concentration in NOI events, which is also supported by the difference in their annual trends between urban and rural areas. The WRF/CMAQ

https://doi.org/10.5194/acp-2022-360
Preprint. Discussion started: 14 June 2022


model and the observed vertical $O_3$ profiles are further applied to illustrate the mechanisms of NOI formation caused by LLJs and Conv. Results confirm that both LLJs and Conv trigger NOI events by inducing downdrafts, the difference being that LLJs induce them by shear and Conv by compensating downdrafts. Through an observational and modeling analysis, this study reveals the long-term (2006-2019) trends of NOI events in the PRD region and quantifies the contribution of meteorological processes for the first time, emphasizing the importance of vertical transport as well as daytime $O_3$ concentration for the occurrence of NOI events.

**Keywords:** Nocturnal ozone increase; Ozone profile; Low-level jets; Convective storms; Pearl River Delta; Long-term trend

## 1 Introduction

As a secondary pollutant, surface ozone($O_3$) is formed via photochemical reactions involving nitric oxide ($NO_x$) and volatile organic compounds (VOCs) in the presence of sunlight. Therefore, $O_3$ shows obvious diurnal variation, with maximum concentrations observed during the day (Kleinman et al., 1994; Zhang et al., 2004). During the night, $O_3$ concentrations are typically low because $O_3$ production ceases, and dry deposition and NO titration directly remove $O_3$ from the atmosphere (Jacob, 2000). However, $O_3$ concentrations do not always stay at low levels during the night, and frequent nocturnal $O_3$ increase (NOI) events have been observed in many countries (Asia, Europe, North America, etc.) and in various topographies (plains, valleys, mountains, etc.) (Kuang et al., 2011; Kulkarni et al., 2013; Klein et al., 2019; Udina et al., 2019; Zhu et al., 2020). Kulkarni et al. (2015) found that NOI events could be observed at around 3:00 in the morning, with concentrations as high as 118 μg $m^{-3}$ in the UK. Yusoff et al. (2019) also reported that frequent NOI events were observed in some cities of Malaysia, and the annual trend was found to be increasing based on 11 years of ground-based measurements. High nocturnal $O_3$ is likely to enhance $O_3$ concentrations the next day and increase the probability of $O_3$ pollution events (Kuang et al., 2011; Sullivan et al., 2017). In addition, numerous studies have proven that high nocturnal surface $O_3$ concentrations have adverse effects on crops and vegetation, leading to plant water loss, stomatal sluggishness, and reduction of plant production (Caird et al., 2007; Cirelli et al., 2016; Yue et al., 2017) and human health (Kurt et al., 2016; Carré et al., 2017).

Because of the cessation of $O_3$ photochemical production at night, NOI events are likely to be attributed to meteorological processes (Salmond and McKendry, 2002). It has been widely recognized that low-level jets (LLJs) are one of the most important meteorological processes that cause NOI events (Salmond and McKendry, 2002; Kuang et al., 2011; Sullivan et al., 2017). After sunset, radiative surface cooling and weakened turbulence result in a stratified nocturnal boundary layer (NBL) with an altitude of about 500m (Stull, 1988). A residual layer (RL) exists above it, which contains the residual $O_3$ produced during the day. When a nighttime LLJ occurs, it is able to break the delamination between the NBL and RL by shear and bring the $O_3$ from the RL to the surface, resulting in the accumulation of ground-level $O_3$. An analysis of aircraft data from California has shown that LLJs are able to promote mixing between the NBL and RL and transport $O_3$ from the RL to the surface, leading to NOI events (Caputi et al., 2019). Convective storms (Conv) are another meteorological process that contributes to NOI events (Prtenjak et al., 2013; Zhu et al., 2020). Dias-Junior et al. (2017) investigated the dynamic variation of $O_3$ during downdrafts associated with Conv and found that these downdrafts play an important role in transporting tropospheric $O_3$ to the surface at night. Jain et al. (2007) noted that NOI events in India are often accompanied by thunderstorms and stable boundary layer conditions. Other meteorological processes that rely heavily on topography, such as sea-land breezes and mountain-valley breezes, also contribute to NOI events (Salmond and McKendry, 2002; Nair et al., 2002). Seibert et al. (2000) pointed out that nocturnal $O_3$ concentrations are elevated during foehn events in the eastern Alps.

Therefore, NOI events are not an exception and can occur worldwide as a result of specific meteorological processes (thunderstorms, foehn, etc.) (Hu et al., 2013; Caputi et al., 2019; Klein et al., 2019; Udina et al., 2019; Shith et al., 2021). LLJs and Conv are important factors influencing the generation of NOI events; however, their relative contribution to NOI events has not yet been quantified. Most of previous studies have focused on the analysis of a single NOI event or NOI events at limited monitoring sites for short periods. Consequently, it is of great important to investigate the long-term trends of NOI events at a larger scale and to further quantify the effect of meteorological processes, such as LLJs and Conv, on NOI events.

China has experienced worsening ground-level $O_3$ pollution in recent years, especially in the Pearl River Delta (PRD) region (Wang et al., 2017). Liao et al. (2021) investigated ozonesonde profiles recorded in Hong Kong during 2000-2019 and pointed out that $O_3$ concentrations have increased substantially at a rate of 0.618 ppbv $yr^{-1}$ in the lower troposphere, indicating the continued deterioration of $O_3$ pollution in

Atmospheric Chemistry and Physics Discussions

the PRD over the last 20 years. The PRD region is the first urban agglomeration in China to change its primary pollution from fine particulate matter with an aerodynamic diameter of less than or equal to 2.5 mm ($PM_{2.5}$) to $O_3$. Numerous studies in the PRD region have explored daytime $O_3$ characteristics, such as long-tern trends (Xue et al., 2014; Li et al., 2022), the nonlinear response to precursor emissions (Lu et al., 2010; Mao et al., 2022), source apportionment (Shen et al., 2015; Liu et al., 2020), and the relative contributions of precursor emissions and meteorology (Yang et al., 2019b; Chen et al., 2020). In terms of nighttime $O_3$, Tong and Leung (2012) analysed diurnal $O_3$ characteristics in different urbanized areas in Hong Kong and found that nocturnal $O_3$ maxima can be higher than daytime maxima in some highly urbanized areas, attributable to differences in NO titration in regions with different urbanization. He et al. (2021) investigated an NOI event at Shaoguan, Guangdong, and revealed that nocturnal mountain-valley breezes from the Nanling Mountains transported $O_3$ from the RL to the surface. However, studies regarding the spatio-temporal distribution of nocturnal $O_3$ concentration and its affecting factors remain unclear in the PRD region. There is an urgent need to comprehensively investigate the characteristics of NOI events in the PRD region because of its special topography, with the coast to the south and the mountains to the north, and because it is frequently affected by special meteorological processes (such as LLJs and Conv) that are conducive to NOI events. Moreover, high daytime $O_3$ concentrations tend to contribute to NOI events in the PRD region.

In this study, by using in-situ hourly $O_3$ concentration data collected from 16 monitoring sites in the PRD region during 2006-2019, the long-term trends and spatial distribution of NOI are presented. Moreover, the relative contributions of LLJs and Conv to NOI events are quantified based on the ERA5 reanalysis dataset. Finally, the observed $O_3$ vertical profile and the Weather Research and Forecasting (WRF) model coupled with the Community Multiscale Air Quality (CMAQ) model are applied to deeply assess the impacts of LLJs and Conv on selected typical NOI events. This study provides a comprehensive analysis of NOI events and their controlling meteorological factors in the PRD region during a 14-year period for the first time, advancing our knowledge of the meteorological role in NOI events.

https://doi.org/10.5194/acp-2022-360
Preprint. Discussion started: 14 June 2022

Atmospheric Chemistry and Physics Discussions
Open Access
EGU

## 2 Data and methods

### 2.1 Observed data

Observed hourly $O_3$ concentrations at 16 stations across the PRD region from 2006 to 2019 are provided by the Guangdong-Hong Kong-Macao Pearl River Delta Regional Air Quality Monitoring Network (HKEPD, 2017) (Fig. 1). More detailed information regarding the stations is provided in Table S1. According to the work of Zhu et al. (2020), a nocturnal $O_3$ increase (NOI) event is defined as $O_3$ concentrations peaking at night (from 21:00 LT to 06:00 LT the next day), with values increasing by at least 10 μg $m^{-3}$ and remaining for at least 1 h. The associated $O_3$ nighttime peak concentration is identified as the nocturnal $O_3$ peak (NOP).

The vertical distribution of $O_3$ concentrations observed at the Dongguan superstation (23.02° N， 113.79° E) during 2019 is also utilized in this study. The $O_3$ vertical profile is measured using an $O_3$ lidar (Model: LIDAR-G-2000). The detection height of the $O_3$ lidar is 3 km, with a vertical spatial resolution of 7.5m and a temporal resolution of 12 min.

The observed meteorological variables at 9 sites (Fig. 1) across the PRD region are obtained from the Chinese National Meteorological Centre (CNMC, http://www.cma.gov.cn/, last accessed on 10 February 2022), including temperature at 2 m (T2), relative humidity at 2 m (RH), and 10 m wind speed (WS10). More detailed information regarding the meteorological sites is provided in Table S2.

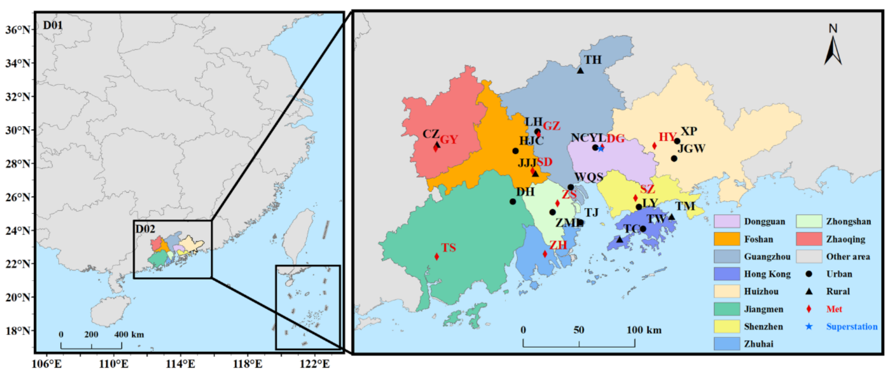


**Figure 1: Model domains and location of air quality monitoring stations (dots and triangles represent urban and rural stations, respectively), meteorological stations (red diamonds), and Dongguan superstation (blue star).**

https://doi.org/10.5194/acp-2022-360
Preprint. Discussion started: 14 June 2022



### 2.2 Simulated meteorological data

To investigate the effects of meteorological processes on NOI events, the ERA5 reanalysis dataset (https://cds.climate.copernicus.eu/cdsapp#!/home, last accessed on 10 February 2022) provided by the European Centre for Medium-Range Weather Forecasts (ECMWF) is utilized in this study. The meteorological parameters include wind speed, precipitation, temperature, and vertical wind velocity. The ERA5 reanalysis dataset, currently spanning from 1979 to the present, is provided on regular latitude–longitude grids at approximately 0.25° × 0.25° and up to 1 h frequency. Vertically, ERA5 resolves the atmosphere using 137 levels from the surface up to a height equalling 0.01 hPa. The performance of ERA5 has been evaluated in previous studies and has proven to be reasonable for further analysis (Olauson, 2018; Hersbach et al., 2020).

Based on the ERA5 reanalysis dataset, low-level jets and convective storms are defined in this study. According to the work of Banta et al. (2002) and Hodges and Pu (2019), low-level jets (LLJs) are defined when vertical wind speed maxima occur below 800hPa and exhibit a decrease of at least 1.5 m $s^{-1}$ at vertical levels both above and below the level of the maxima.

Convective storms (Conv) are defined by the following criterion: the mean K index (KI) value is greater than 30 ℃ within 3 hours prior to the NOI event (George, 1960; Johnson, 1982). The KI is calculated as follows:

$$KI = (T_{850} - T_{500}) + Td_{850} - (T_{700} - Td_{700}) \quad (1)$$

where $T_{850}$, $T_{700}$, and $T_{500}$ are the temperature at 850 hPa, 700 hPa, and 500 hPa, respectively, and $Td_{850}$ and $Td_{700}$ are the dew point temperature at 850 hPa and 700 hPa, respectively.

### 2.3 Model configuration

The Weather Research and Forecasting (WRFv3.9.1) model is applied to provide meteorological inputs to drive the Community Multiscale Air Quality (CMAQ v5.3.1) model. The meteorological initial conditions (IC) and boundary conditions (BC) are provided by the National Centers for Environmental Prediction (NCEP) Final Analyses (FNL) dataset, with a spatial resolution of 1° × 1° and a temporal resolution of 6 h. The main physics options used for the WRF model are shown in Table 1. Two-nested domains are used in the WRF simulations, with 38 vertical layers from the surface to 100 hPa. Figure 1 shows the two nested modelling domains, with spatial resolutions of 27 km × 27 km and 3 km × 3 km

https://doi.org/10.5194/acp-2022-360
Preprint. Discussion started: 14 June 2022


Atmospheric Chemistry and Physics Discussions

for the coarse (D01) and inner (D02) domains, respectively. D01 covers most regions of China and D02 covers the whole PRD region.

The CMAQ model is explored to simulate $O_3$ concentrations in the PRD region. The SAPRC07 and AERO6 aerosol module are used for gas-phase and particulate matter chemical mechanisms, respectively (Carter, 2010; Wyat Appel et al., 2018). Chemical IC and BC for D01 are derived from a global chemical transport model, the Model for Ozone and Related chemical Tracers, version 4 (MOZART4) (Emmons et al., 2010), and those for D02 are provided by the simulated results from D01. The anthropogenic emissions for D01 are based on the 2016 Multi-resolution Emission Inventory for China (MEIC), which has a grid resolution of 0.25° × 0.25° (Zheng et al., 2018). Those used for D02 are based on the 2017 high-resolution emission inventory of the PRD region with a grid resolution of 3 km × 3 km (Zhong et al., 2018), which includes the emission sectors of agriculture, biomass burning, combustion, dust, industrial process, nonroad, solvent, storage, transportation, and waste disposal sources. Biogenic emissions are calculated by the Model of Emissions of Gases and Aerosols from Nature (MEGAN) v2.1 (Guenther et al., 2006; Wang et al., 2011).

**Table 1. Model configurations**

| Model | Physical process | Parameterization scheme | Reference |
|---|---|---|---|
| WRF | Microphysics | Lin | Lin et al. (1983) |
| | Longwave radiation | RRTMG | Iacono et al. (2008) |
| | Shortwave radiation | RRTMG | Iacono et al. (2008) |
| | Surface layer | Monin-Obukhov | Monin and Obukhov (1954) |
| | Planetary boundary layer | MYJ | Nakanishi and Niino (2006) |
| | Cumulus parameterization | Grell-3 | Grell and Dévényi (2002) |
| | Land surface | Noah land-surface model | Chen and Dudhia (2001) |
| CMAQ | Gas-phase chemistry | SAPRC 07 | Carter (2010) |
| | Aerosol chemistry | AERO6 | Carlton et al. (2010) |

### 2.4 Process analysis

In this work, in order to interpret the underlying atmospheric mechanisms for NOI events, the Integrated Process Rates (IPR) analysis tool embedded in the CMAQ model is used to identify and quantify the

Atmospheric Chemistry and Physics Discussions

contribution of different physical and chemical processes to $O_3$. The processes include horizontal transport (HTRA), vertical transport (VTRA), gas-phase chemistry (CHEM), dry deposition (DDEP), and cloud processes (CLDS). Horizontal transport is the sum of horizontal advection and diffusion, and vertical transport is the sum of vertical advection and diffusion. More details regarding the IPR analysis tool can be found in previous works (Liu et al., 2010; Wang et al., 2010).

Using the CMAQ-IPR model, a NOI event induced by LLJs that occurred at the Nancheng Yuanling (NCYL) site in Dongguan on 13-14 September 2017 is selected as a typical case for further analysis. The simulations are conducted during 6-14 September. The first 2 days are used as model spin-up to eliminate the impact of IC (Jiménez et al., 2007).

### 2.5 Model evaluation

The WRF/CMAQ simulation results are evaluated by comparing with the available ground-based observation. Statistical metrics including mean value ($\overline{Obs}$ and $\overline{Sim}$), mean bias (MB), normalized mean bias (NMB), normalized mean error (NME), root mean square error (RMSE), correlation coefficient (r), and index of agreement (IoA), are calculated as follows to evaluate model performance.

$$MB = \overline{Obs} - \overline{Sim} \qquad (1)$$

$$NMB = \frac{\sum_{i=1}^{n}(Sim_i - Obs_i)}{\sum_{i=1}^{n} Obs_i} \times 100 \qquad (2)$$

$$NME = \frac{\sum_{i=1}^{n}|Sim_i - Obs_i|}{\sum_{i=1}^{n} Obs_i} \times 100 \qquad (3)$$

$$RMSE = \sqrt{\frac{1}{n}\sum_{i=1}^{n}(Sim_i - Obs_i)^2} \qquad (4)$$

$$r = \frac{\sum_{i=1}^{n}(Sim_i - \overline{Sim})(Obs_i - \overline{Obs})}{\sqrt{\sum_{i=1}^{n}(Sim_i - \overline{Sim})^2 \sum_{i=1}^{n}(Obs_i - \overline{Obs})^2}} \qquad (5)$$

$$IoA = 1 - \frac{\sum_{i=1}^{n}(Sim_i - Obs_i)^2}{\sum_{i=1}^{n}\left(|Sim_i - \overline{Obs}| + |Obs_i - \overline{Obs}|\right)^2} \qquad (6)$$

The evaluation protocols of the U.S. Environmental Protection Agency (EPA, 2017) are used to evaluate the performance of the meteorological parameters, which are listed as follows: MB ≤ ±0.5 °C and IoA ≥ 0.8 for T2; MB ≤ ±5 % and IoA ≥ 0.6 for RH; and MB ≤ ±0.5 m/s, RMSE ≤ 2.0 m/s, and IoA ≥ 0.6 for WS10. The evaluation protocols of the Ministry of Environmental Protection of China (MEP, 2015) are used to evaluate the performance of $O_3$ as follows: −15 % < NMB < 15 %, NME < 35 %, and r > 0.4.

https://doi.org/10.5194/acp-2022-360
Preprint. Discussion started: 14 June 2022




## 3 Results and discussion

### 3.1 General characteristics of NOI events

The annual average frequency of NOI events is estimated to be 53 ± 16 d $yr^{-1}$ in the PRD region from 2006 to 2019, with an annual average concentration of 58 ± 11 μg $m^{-3}$ for NOP. LLJs are the primary factor causing NOI events, responsible for about 61 %, followed by Conv at 11 % (Fig. 2). The combination of LLJs and Conv contributes to 16 % of NOI events. The remaining 12 % of NOI events that cannot be explained by LLJs and Conv may be related to other meteorological processes, such as mountain-valley breezes and sea-land breezes (Sousa et al., 2011; He et al., 2021).

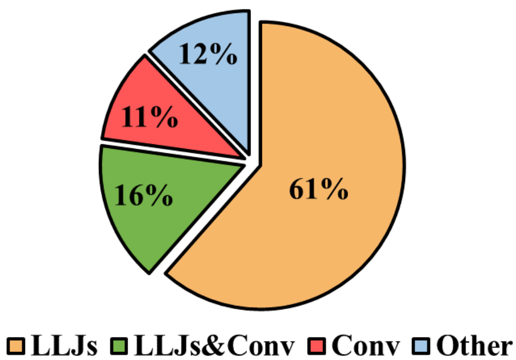


**Figure 2: The relative contribution of different meteorological processes to NOI events.**

### 3.2 Long-term trends of NOI events

As depicted in Fig. 3a, the annual frequency of NOI events increases from 38 ± 18 d $yr^{-1}$ in 2006 to as high as 67 ± 18 d $yr^{-1}$ in 2011 at a rate of 4.70 d $yr^{-1}$ ($p<0.01$) and gradually decreases at a rate of -0.72 d $yr^{-1}$ ($p<0.05$) after 2012. A similar annual trend is observed between the frequency of total downdrafts (sum of LLJs, LLJs + Conv, and Conv) and NOI events (Fig. 3b). The frequency of total downdrafts increases at a rate of 4.02 d $yr^{-1}$ ($p<0.01$) before 2012 and decreases at a rate of -0.53 d $yr^{-1}$ ($p<0.05$) afterward, which is significantly positively correlated with NOI events, with a Pearson correlation coefficient (r) of 0.96 ($p<0.01$). Among the total downdrafts, LLJs exhibit a similar pattern with NOI events ($r=0.89$, $p<0.01$), further suggesting that LLJs are the predominant driver. Conv presents a continuously increasing trend over the whole 14-year period, with a rate of 0.26 d $yr^{-1}$ ($p<0.01$), and the frequency of LLJs + Conv does not show obvious variation.

Although the proportion of NOI events caused by Conv alone is relatively small compared with that caused by LLJs (Fig. 2), it is noteworthy that the frequency of Conv-induced NOI events gradually

https://doi.org/10.5194/acp-2022-360
Preprint. Discussion started: 14 June 2022




increases during the 14-year period (Fig. 3b). This is related mostly to the rapid urbanization in the PRD in recent years. During 1987-2017, the urban area of the PRD region grew at an average rate of 8.82 % $yr^{-1}$ (Yang et al., 2019a) and reached its maximum rate (6.66 %) of urban expansion intensity after 2010 (Zhang et al., 2021). These expanding urban areas increase surface roughness and further increase the frequency and intensity of convection in the form of enhanced mechanical turbulence (Li et al., 2021), resulting in the enhanced frequency of Conv-induced NOI events. The role of Conv in the occurrence of NOI events is expected to amplify as the trend toward urbanization continues in China in the future (Seto et al., 2012; Marelle et al., 2020).

Unlike the annual trend of NOI frequency, the nocturnal $O_3$ peak (NOP) value shows an upward trend during the period 2006-2019, with a slower growth rate of 0.54 μg $m^{-3}$ $yr^{-1}$ ($p<0.05$) before 2015 and a faster growth rate of 4.76 μg $m^{-3}$ $yr^{-1}$ ($p<0.01$) thereafter (Fig. 3c). The maximum daily average 8-h (MDA8) $O_3$ mixing ratio exhibits a similar pattern to NOP, with an increase rate of 0.39 μg $m^{-3}$ $yr^{-1}$ ($p<0.05$) before 2015 and 9.21 μg $m^{-3}$ $yr^{-1}$ ($p<0.01$) afterward (Fig. 3d). NOP is significantly positively correlated with MDA8 $O_3$, with r up to 0.88 ($p<0.01$). This implies that daytime $O_3$ concentration levels potentially affect NOP concentrations. Previous studies have pointed out that weakened NO titration caused by the effective control of anthropogenic $NO_x$ emissions, coupled with the rapid increase in VOCs emissions in the PRD region (Zhong et al., 2018), caused the increasing $O_3$ concentrations in the past 14 years (Ma et al., 2016; Liao et al., 2021; Li et al., 2022). Moreover, some studies have reported increasing atmospheric oxidizing capacity in the PRD region in recent years, which is considered to be an important contributor to accelerated $O_3$ growth during 2016-2019 (Gong et al., 2018; Han et al., 2019). The weakened NO titration not only increases the daytime $O_3$ concentration, but also allows more unconsumed $O_3$ to enter the RL after sunset, leading to more downward transport of $O_3$ during NOI events. This has also been shown by Tong and Leung (2012), who emphasized that significant variation in NO titration levels and the diurnal accumulation of tropospheric $O_3$ can seriously affect nighttime $O_3$ concentrations.

https://doi.org/10.5194/acp-2022-360
Preprint. Discussion started: 14 June 2022



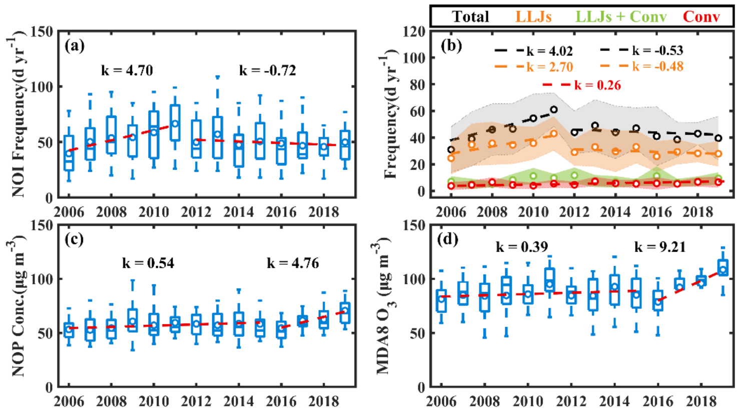


**Figure 3: Annual trends of (a) NOI event frequency, (b) frequency of total downdrafts (black), LLJs (orange), LLJs + Conv (green), and Conv (red) that can induce NOI events, (c) NOP concentrations, and (d) MDA8 $O_3$ concentrations in the PRD region during 2006-2019. The units of k (Sen's Slope) are d$^{-1}$ yr$^{-1}$ in (a) - (b) and μg m$^{-3}$ yr$^{-1}$ in (c) - (d). Linear trends significant at the 95% confidence level are illustrated with dashed lines.**

### 3.3 Seasonal variations of NOI events

NOI events exhibit obvious seasonal variation (Fig. 4a), with relatively higher frequency observed in spring (18 ± 4 d yr$^{-1}$) and autumn (20 ± 5 d yr$^{-1}$) and lower frequency in summer (14 ± 3 d yr$^{-1}$) and winter (16 ± 3 d yr$^{-1}$). LLJs are the dominant inducer of NOI events in spring, autumn, and winter (Fig. 4b), while in summer, the dominant factors are LLJs + Conv and Conv because convective activity is more intense during summer (Chen et al., 2014). Given that LLJs can enhance turbulence below and create favorable formation conditions for Conv (Trier et al., 2017; Du and Chen, 2019), most Conv events occur preferentially on days when LLJs exist in the PRD region (Chen et al., 2014), which makes LLJs + Conv the primary contributor in summer.

In terms of NOP (Fig. 4c), relatively higher concentration is observed in spring and autumn, with values of 59 ± 12 μg m$^{-3}$ and 66 ± 10 μg m$^{-3}$, respectively, while the concentration is the lowest (44 ± 7 μg m$^{-3}$) in summer. The MDA8 $O_3$ has a similar seasonal variation to NOP except in winter (Fig. 4d); it is high in the spring (111 ± 15 μg m$^{-3}$) and autumn (120 ± 13 μg m$^{-3}$) and low in the summer (88 ± 15 μg m$^{-3}$). In winter, surface MDA8 $O_3$ has the lowest concentration (86 ± 12 μg m$^{-3}$) while NOP stays at relatively high levels (56 ± 10 μg m$^{-3}$). This is because the higher $O_3$ concentrations aloft in the winter allow more $O_3$ to be transported downward during the NOI period, resulting in a higher NOP concentration in winter, which shown by the seasonal observed vertical $O_3$ profile monitored at the Dongguan superstation (Fig. 5). As illustrated in Fig. 5, higher $O_3$ concentrations are observed at the height of 200 to 750 m in the

https://doi.org/10.5194/acp-2022-360
Preprint. Discussion started: 14 June 2022



winter compared to summer, and a similar result was also observed in Hong Kong (Liao et al., 2021). This is owing mainly to the typical Asian monsoon circulation, because it can bring clean marine air into the PRD region in summer, which dilutes polluted air masses inland, and delivers pollutant-laden air from mainland China in winter, creating higher $O_3$ concentrations over the PRD (Wang et al., 2009).

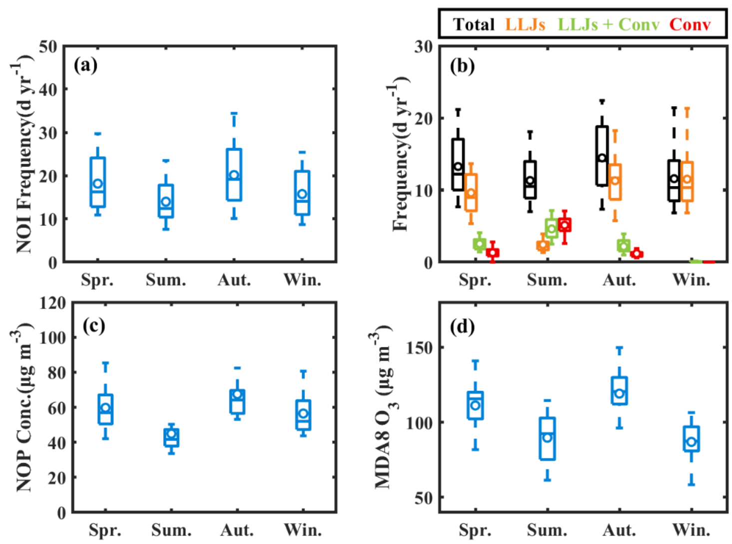


**Figure 4: Seasonal variation of (a) NOI event frequency, (b) frequency of total downdrafts (black), LLJs (orange), LLJs + Conv (green), and Conv (red) that can induce NOI events, (c) NOP concentrations, and (d) MDA8 $O_3$ concentrations in the PRD region during the period 2006-2019.**

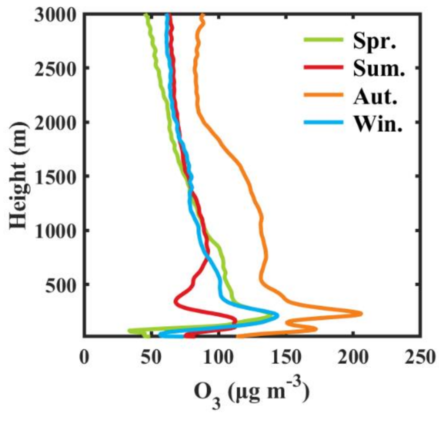


**Figure 5: Seasonally averaged vertical distribution of $O_3$ concentrations at the Dongguan superstation from the surface to a height of 3000 m during 2019. Spring (Spr.): March-May; Summer (Sum.): June-August; Autumn (Aut.): September-November; Winter (Win.): December-February.**

### 3.4 Diurnal variation of NOI events

Distinct diurnal variation is observed for NOI events (Fig. 6a) with an increasing trend from 21:00 to 3:00 and a decreasing trend afterward. It is estimated that about 60 % of events occur during the middle of the night (11:00-3:00). The LLJs that can induce NOI events show a similar diurnal variation to the frequency of NOI events, occurring frequently at midnight. However, the frequency of total LLJs differs from the frequency of LLJs that can induce NOI events, increasing continuously from 21:00 to 0:00 and remaining stable after 0:00. This suggests that LLJs are not the only factor that determines whether a NOI event can develop. The other decisive factor is related to $O_3$ concentrations in the RL. During 21:00-3:00, $O_3$ produced during the day enters the RL and remains at a relatively high level. During this period, the occurrence of LLJs tends to increase the probability of NOI events. After 3:00, the $O_3$ concentrations in the RL decrease due to horizontal and vertical transport during 21:00-3:00, which reduces the amount of $O_3$ that can be transported downward. Hance, even though the frequency of LLJs is relatively high after 3:00, the lower $O_3$ in the RL results in less $O_3$ being transported downward to form a NOI event, which ultimately decreases the frequency of NOI events. As illustrated in Fig. 6c, the trends of NOP concentrations from 21:00 to 6:00 also reflect the fact that $O_3$ concentrations in the RL are higher during 21:00-0:00 and lower during 0:00-6:00. Therefore, the development of a NOI event is influenced by the combination of a downdraft induced by meteorological processes, and daytime $O_3$ concentrations.

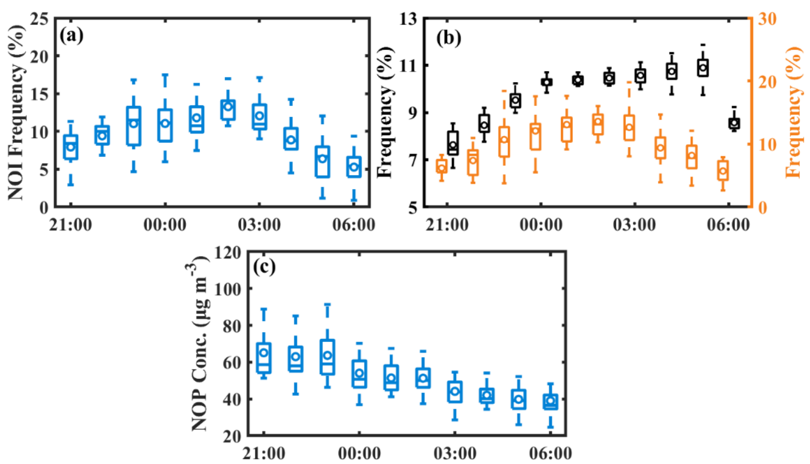


**Figure 6: Diurnal variation of (a) NOI event frequency, (b) frequency of total LLJs (black) and the LLJs that can induce NOI events (blue), (c) NOP concentrations during 21:00-06:00 (LTC).**

https://doi.org/10.5194/acp-2022-360
Preprint. Discussion started: 14 June 2022



### 3.5 Spatial distribution of NOI events

As most NOI events are caused by LLJs, LLJs are taken as an example to study the role of meteorological processes in the spatial distribution of NOI events. The spatial distribution of the average annual frequency of NOI events and LLJs in the PRD from 2006 to 2019 is shown in Fig. 7a, and the spatial distribution of MDA8 $O_3$ concentrations obtained by Kriging's interpolation method is shown in Fig. 7b. Obvious geographical variation is observed for NOI events, with a higher frequency in the eastern PRD region, coupled with a higher frequency of LLJs, although the MDA8 $O_3$ concentrations are relatively lower in these regions. In the central PRD region, despite the highest MDA8 $O_3$ concentrations, the frequency of NOI events was the lowest.

To further elaborate the effect of meteorological processes and daytime $O_3$ concentrations on NOI events, the difference between annual trends in urban and rural areas is compared in Fig. 8. This shows that the frequency of NOI events exhibits an increasing trend in both urban and rural areas during 2006-2011, with a faster rate of increase in urban areas (0.49) than in rural areas (0.11). The increase in NOI events in urban and rural areas during 2006-2011 is associated with the increase in both LLJ frequency and MDA8 $O_3$ concentration. In 2012-2019, NOI events remain stable in urban areas (0.02) because of the decrease in the frequency of LLJs in urban areas, even though MDA8 $O_3$ increases (0.26). In rural areas, the frequency of NOI events decreases (-0.17) during 2012-2019 because of the decrease in the frequency of LLJs coupled with the stabilization of MDA8 $O_3$, leading to fewer NOI events. This emphasizes the more important role of vertical transport induced by meteorological processes in the formation of NOI events.

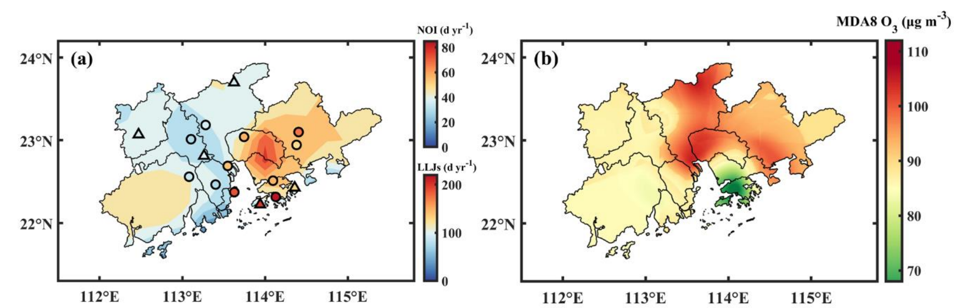


**Figure 7: Spatial distribution of annual average (a) NOI event frequency (points) and LLJs frequency (contours), (b) MDA8 $O_3$ concentrations. The dots and triangles represent urban and rural stations, respectively.**

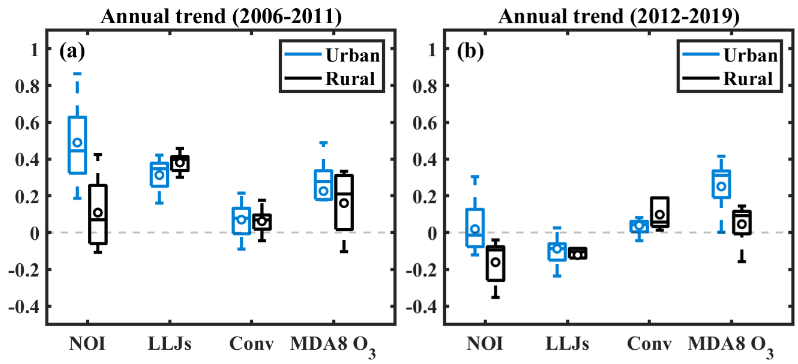


**Figure 8: The normalized annual trend in the frequency (or concentration) of NOI events, LLJs, Conv, and MDA8 $O_3$ for urban and rural areas in the PRD region for the period of (a) 2006-2011 and (b) 2012-2019.**

### 3.6 Causative analysis of NOI events: Convective storms trigger

In order to elaborate the underlying atmospheric mechanisms for Conv-induced NOI events, a distinct $O_3$ increase associated with Conv observed at the Nancheng Yuanling (NCYL) site in Dongguan on 3-4 September 2019 is taken as a typical example for deeper discussion. The vertical $O_3$ profile data observed at the Dongguan superstation are used to represent the vertical $O_3$ distribution at the NCYL site since the distance between these two stations is only 3 km.

As shown in Fig. 9a, the KI remains above 36 ℃ from 14:00 to 23:00, indicating a high possibility of convection. Meanwhile, the vertical velocity results show a continuous and strong updraft at 1-3 km altitude during the afternoon (Fig. 9b), which confirms the occurrence of convection. Subsequently, a convective precipitation event occurs during 16:00-20:00. The effect of rainfall on $O_3$ removal is relatively small after sunset, because wet deposition of $O_3$ occurs through the removal of the precursors $HNO_3$ and $H_2O_2$ by water vapor under solar radiation, which is indirect and rather peripheral, and the effect of heterogeneous processes on $O_3$ removal is weak (Jacob, 2000; Awang et al., 2015; Zhu et al., 2020). Therefore, the unconsumed $O_3$ is allowed to enter the RL and remains stable. As illustrated in Fig. 9c, higher $O_3$ concentrations are found in the RL after 18:00, reaching around 200 μg $m^{-3}$. At 21:00, a strong updraft suddenly appears above 1.5 km, which subsequently causes a strong compensating downdraft below 1 km at around 23:00. The downdraft breaks the stable nocturnal boundary layer and transports the $O_3$ from the RL to the surface (Fig. 9c). Hence, the NOI event occurs at 23:00, with $O_3$ concentrations increasing from 45 μg $m^{-3}$ at 22:00 to 59 μg $m^{-3}$ at 23:00.

https://doi.org/10.5194/acp-2022-360
Preprint. Discussion started: 14 June 2022

Atmospheric Chemistry and Physics
Open Access
EGU
Discussions

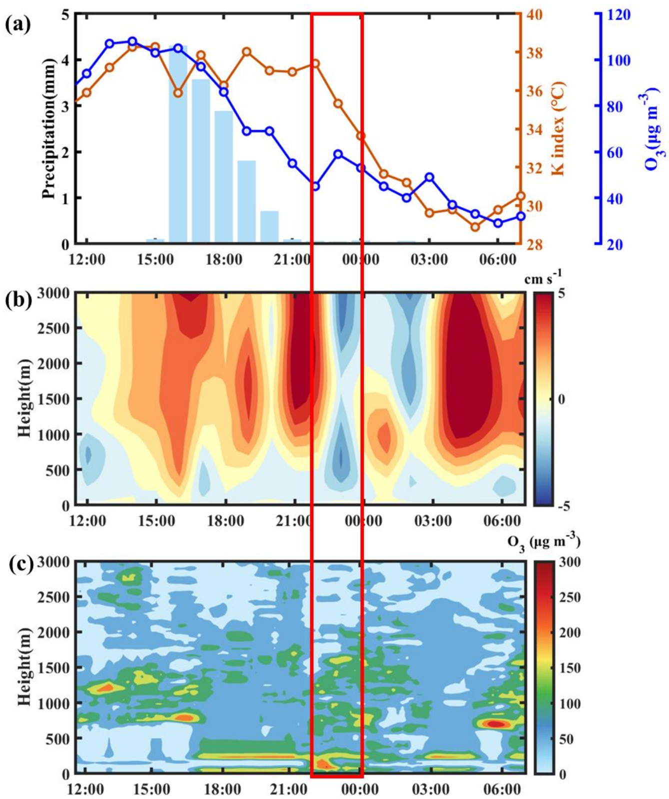


**Figure 9: An NOI event occurred at NCYL site in Dongguan on 3-4 September 2019. (a) Hourly variations of KI (brown line), $O_3$ concentrations (blue line), and hourly precipitation amount (blue bar), (b) vertical wind velocity, with positive and negative values related to updrafts and downdrafts, (c) vertical profile of $O_3$ concentrations as measured by $O_3$ lidar.**

### 3.7 Causative analysis of NOI events: LLJ trigger

Another typical NOI event induced by LLJs occurred at the NCYL site in Dongguan on 13-14 September 2017 and is simulated by the CMAQ-IPR model due to the lack of observed vertical profiles of wind speed and $O_3$ concentrations. Model performance is first evaluated. Comparisons of simulated meteorological parameters with hourly observations for the 9 sites in the PRD region during 8-14 September 2017 are shown in Fig. S1, with statistical indices reported in Table S3. The results show that WS10 is reasonably well simulated, as the MB, RMSE, and IoA of the regional average meet the criteria. The simulated RH and T2 of the regional average are slightly overestimated (MB=-6.1 %) and underestimated (MB=1.4 °C), respectively, while they perform well at the Dongguan site, where both

https://doi.org/10.5194/acp-2022-360
Preprint. Discussion started: 14 June 2022




the MB (RH=-1.0 %, T2=0.5 °C) and IoA (both are 1.0) meet the criteria. The MB of the simulated WS10 in Dongguan site is slightly underestimated (MB=0.7 m $s^{-1}$), but the RMSE and IoA meet the criteria. Comparisons of simulated $O_3$ with hourly observations during 8-14 September 2017 are shown in Fig. S1, with statistical indices reported in Table S4. The simulated $O_3$ shows a good performance in the PRD region, with NMB (-4.8 %), NME (17.7 %) and r (1.0) all meeting the criteria, while it is slightly underestimated at the NCYL site in Dongguan but still meets the criteria (NMB=-12.7 %, NME=29.8 %, r=0.8). Therefore, the simulation results of the meteorological parameters and $O_3$ are reasonable and reliable for further analysis.

Figure 10a shows the time series of simulated $O_3$ concentrations and the contributions of different processes to surface $O_3$ concentrations at the NCYL site in Dongguan during 13-14 September 2017. During the night on 13 September, $O_3$ concentrations increase from 45 μg $m^{-3}$ at 21:00, peak at 85 μg $m^{-3}$ at around 22:00, and fall to 15 μg $m^{-3}$ at 00:00. Prior to 21:00, the magnitude of the negative contribution of chemical processes to $O_3$ is greater than the positive contribution of vertical transport, resulting in net $O_3$ depletion. This suggests that gas-phase chemistry processes such as NO titration are the main pathway for $O_3$ loss at night. At 21:00, the vertical and horizontal transport contribution increase abruptly by 48 μg $m^{-3}$ and 27 μg $m^{-3}$, respectively, while the chemical depletion remains constant. At this point, the net $O_3$ concentration turns from loss to production (51 μg $m^{-3}$). In terms of vertical distribution (Fig. 10b), a positive contribution of both vertical and horizontal transport can be found at the surface, while vertical transport become negative in the upper layers and horizontal transport remains positive, indicating the occurrence of a downdraft. In addition, the wind profile shows a typical LLJ characteristic (Fig. 10b), with a maximum wind speed of about 12 m $s^{-1}$ at the height of 1 km and a wind speed difference of more than 3 m $s^{-1}$ above and below. Figure 11 further presents the process of vertical transport during an NOI event. Compared to normal days, the nocturnal boundary layer during the NOI event is more unstable and turbulent, with significant upward and downward transport. At around 1 km, there is a straight stream over the NCYL site during the NOI event (Fig. 11b). This suggests that LLJs break the stable structure between the nocturnal boundary layer and the RL and enhance the strength of turbulence (Caputi et al., 2019). The LLJ-induced turbulence promotes mixing between the upper and lower layers and continuously transports $O_3$ from the upper layer to the surface, causing an unusual surge in $O_3$ at the surface and leading to a NOI event. As a result, the LLJ process contributes as much as 40 μg $m^{-3}$ $O_3$ from the upper layer to the surface during this NOI event.

https://doi.org/10.5194/acp-2022-360
Preprint. Discussion started: 14 June 2022


Atmospheric Chemistry and Physics
Discussions
Open Access
EGU

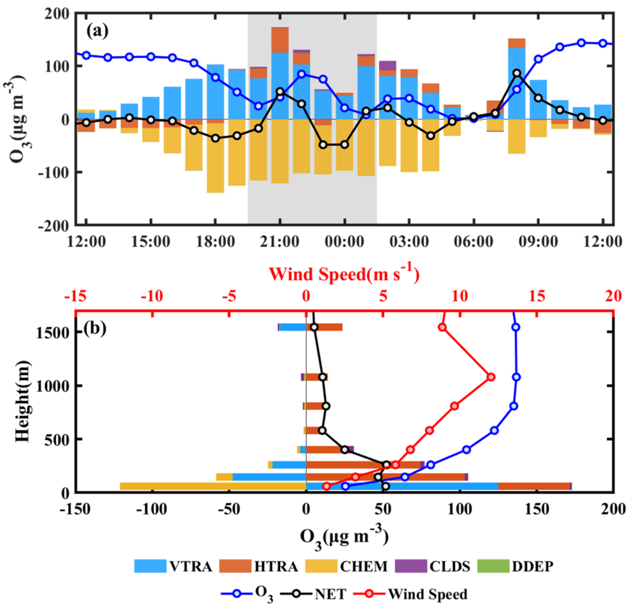


**Figure 10: Contribution of individual processes to (a) hourly $O_3$ concentration near the surface during 13-14 September 2017 and (b) vertical $O_3$ concentration at 21:00 on 13 September 2017. (VTRA: vertical transport, the net effect of vertical advection and diffusion; HTRA: horizontal transport, the net effect of horizontal advection and diffusion; CHEM: gas-phase chemistry; CLDS: cloud processes; DDEP: dry deposition; NET: the net change in $O_3$ due to all atmospheric processes; the red line represents the wind speed in the vertical direction).**

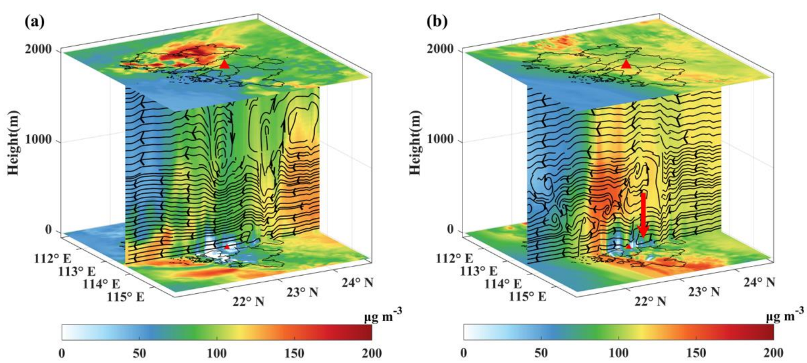


**Figure 11: Vertical profiles of $O_3$ concentrations at 21:00 during (a) a normal day (12 September 2017) and (b) a NOI event (13 September 2017). Red triangles represent the NCYL site in Dongguan, contours represent $O_3$ concentrations ($\mu g\ m^{-3}$), and black lines and arrows indicate airflow and its direction.**

### 3.8 Comparison and Prospects

Zhu et al. (2020) identified a NOI event frequency of 16-19 d $yr^{-1}$ during summer from 2014 to 2015 in Beijing, China, with nocturnal $O_3$ maxima ranging from 45 to 85 μg $m^{-3}$, which is comparable to our result of NOI frequency (14 ± 3 d $yr^{-1}$) and slightly higher than our NOP concentration (44 ± 7 μg $m^{-3}$) in summer. Sousa et al. (2011) analyzed nocturnal $O_3$ maxima events (maxima higher than the average nocturnal $O_3$ concentration of 10 μg $m^{-3}$) during 2005-2007 in northern Portugal and found that the frequencies of nocturnal $O_3$ maxima were between 40% and 50% in urban areas and 15% in rural areas, which is higher than our NOI frequency (53 d $yr^{-1}$, 14.5%). Other studies focusing on short-term nocturnal $O_3$ maxima cases found that NOP concentrations were 30-50 μg $m^{-3}$ in the Lower Fraser Valley, British Columbia Canada (Salmond and McKendry, 2002), 20-60 μg $m^{-3}$ in Senegal (Grant et al., 2008), and 40-80 μg $m^{-3}$ in north America (Kuang et al., 2011; Hu et al., 2013; Sullivan et al., 2017), values that are comparable to our results (58 ± 11 μg $m^{-3}$).

Our study emphasizes the importance of meteorological processes as well as daytime $O_3$ concentration in the occurrence of NOI events, implying that higher NOP may occur during a severe daytime $O_3$ pollution period under the effect of meteorological processes. The occurrence of NOI events is likely to improve the next day's chemical budget and increase the probability of $O_3$ pollution events, which makes $O_3$ prevention more complex and challenging (Ravishankara, 2009; Sullivan et al., 2017). However, the relationship between NOI events and the following daytime $O_3$ pollution remains unclear and controversial. Klein et al. (2019) found lower $O_3$ pollution levels on the day following NOI events, while Kuang et al. (2011) and Sullivan et al. (2017) found a higher increasing rate of $O_3$ and poorer air quality on the following day. Deeper analyses are needed in the future to explore the relationship between daytime and nighttime $O_3$ pollution under the effect of vertical transport.

## 4 Conclusion

In this study, based on in-situ $O_3$ concentrations, observed $O_3$ vertical profiles, ERA5 reanalysis datasets, and the WRF-CMAQ model, the spatial and temporal characteristics of NOI events are comprehensively presented and the role of vertical transport in NOI events is further quantified in the PRD region from 2006 to 2019.

https://doi.org/10.5194/acp-2022-360
Preprint. Discussion started: 14 June 2022




The annual average frequency of NOI events is estimated to be 53 ± 16 d $yr^{-1}$ from 2006 to 2019, with an annual average of 58 ± 11 μg $m^{-3}$ for the nocturnal $O_3$ peak (NOP). Low-level jets (LLJs) and convective storms (Conv) are identified as the two main factors causing NOI events, with 61 % and 11 % of NOI events induced by LLJs and Conv, respectively. A high correlation between NOI events and LLJs frequency rather than Conv in the annual trend ($r=0.89$, $p<0.01$) supports the high contribution of LLJs. Although the contribution of Conv to NOI events is relatively small, Conv-induced NOI events continuously increased at a rate of 0.26 d $yr^{-1}$ during this 14-year period owing to the effect of expanding urbanization. Moreover, the good agreement between NOP and maximum daily average 8-h (MDA8) $O_3$ in annual ($r=0.88$, $p<0.01$) and seasonal trends ($r=0.80$, $p<0.01$) and a higher NOI frequency (60%) during the first half of the night imply that daytime $O_3$ concentrations are also an important factor influencing the formation of NOI events. In addition, a more important role of vertical transport induced by meteorological processes in the formation of NOI events has been demonstrated by a good consistent spatial distribution between NOI events and LLJs frequency rather than MDA8 $O_3$, and by the difference in annual trends between urban and rural areas.

Two typical NOI events caused by LLJs and Conv, respectively, further demonstrate that downdrafts from enhanced turbulence are the direct cause of NOI events, as these can carry $O_3$ from the RL to the surface. The difference is that LLJs induce downdrafts by a fast-moving air mass enhancing shear below, whereas Conv induce downdraft by compensating downdrafts.

This study emphasizes the role of vertical transport induced by meteorological processes and daytime $O_3$ concentration in the formation of NOI events and highlights a more important contribution of vertical transport in linking daytime and nighttime $O_3$ pollution. This study not only provides a new perspective and advanced understanding to reconceptualize the role of meteorology in daytime and nighttime $O_3$ pollution, but also provides a reference for other regions facing ground-level $O_3$ pollution.

*Data availability.* In-situ hourly $O_3$ concentrations at 16 stations across the PRD region from 2006 to 2019 can be downloaded from http://113.108.142.147:20047; the observed hourly meteorological data at the 9 sites across the PRD region can be downloaded from http://www.cma.gov.cn/; the ERA5 reanalysis dataset can be downloaded from https://cds.climate.copernicus.eu/cdsapp#!/home; and the vertical $O_3$ profile data available upon request.

*Author contributions.* YW and WC designed the research. YW did the data analysis and simulation work and prepared the draft with support and editing from WC. YY and QX contributed to data analysis. SJ and XW contributed to paper revision.

*Competing interests.* The authors declare that they have no conflict of interest.

*Acknowledgements.* This study was supported by the Key-Area Research and Development Program of Guangdong Province(2020B1111360003), the National Natural Science Foundation of China (41905086, 42121004, 41905107, 42077205, 41425020), the National Key Research and Development Plan (2019YFE0106300), the Special Fund Project for Science and Technology Innovation Strategy of Guangdong Province (2019B121205004), the AirQuip (High-resolution Air Quality Information for Policy) Project funded by the Research Council of Norway, the Collaborative Innovation Center of Climate Change, Jiangsu Province, China, and the high-performance computing platform of Jinan University.

## References

Awang, N. R., Ramli, N. A., Yahaya, A. S., and Elbayoumi, M.: High nighttime ground-level ozone concentrations in Kemaman: NO and NO2 concentrations attributions, Aerosol Air Qual. Res., 15, 1357-1366, https://doi.org/10.4209/aaqr.2015.01.0031, 2015.

Banta, R. M., Newsom, R. K., Lundquist, J. K., Pichugina, Y. L., Coulter, R. L., and Mahrt, L.: Nocturnal low-level jet characteristics over Kansas during CASES-99, Boundary-Layer Meteorol., 105, 221-252, https://doi.org/10.1023/A:1019992330866, 2002.

Caird, M. A., Richards, J. H., and Donovan, L. A.: Nighttime stomatal conductance and transpiration in C3 and C4 plants, Plant Physiol., 143, 4-10, https://doi.org/10.1104/pp.106.092940, 2007.

Caputi, D. J., Faloona, I., Trousdell, J., Smoot, J., Falk, N., and Conley, S.: Residual layer ozone, mixing, and the nocturnal jet in California's San Joaquin Valley, Atmos. Chem. Phys., 19, 4721-4740, https://doi.org/10.5194/acp-19-4721-2019, 2019.

https://doi.org/10.5194/acp-2022-360
Preprint. Discussion started: 14 June 2022


Carlton, A. G., Bhave, P. V., Napelenok, S. L., Edney, E. O., Sarwar, G., Pinder, R. W., Pouliot, G. A., and Houyoux, M.: Model representation of secondary organic aerosol in CMAQv4.7, Environ. Sci. Technol., 44, 8553-8560, https://doi.org/10.1021/es100636q, 2010.

Carré, J., Gatimel, N., Moreau, J., Parinaud, J., and Leandri, R.: Influence of air quality on the results of in vitro fertilization attempts: A retrospective study, Eur. J. Obstet. Gynecol. Reprod. Biol., 210, 116-122, https://doi.org/10.1016/j.ejogrb.2016.12.012, 2017.

Carter, W. P. L.: Development of the SAPRC-07 chemical mechanism, Atmos. Environ., 44, 5324-5335, https://doi.org/10.1016/j.atmosenv.2010.01.026, 2010.

Chen, F. and Dudhia, J.: Coupling an advanced land surface–hydrology model with the Penn State–NCAR MM5 modeling system. Part I: Model implementation and sensitivity, 129, 569-585, https://doi.org/10.1175/1520-0493(2001)129<0569:CAALSH>2.0.CO;2, 2001.

Chen, X., Zhao, K., and Xue, M.: Spatial and temporal characteristics of warm season convection over Pearl River Delta region, China, based on 3 years of operational radar data, J. Geophys. Res. Atmos., 119, 12,447-465, https://doi.org/10.1002/2014jd021965, 2014.

Chen, X., Zhong, B., Huang, F., Wang, X., Sarkar, S., Jia, S., Deng, X., Chen, D., and Shao, M.: The role of natural factors in constraining long-term tropospheric ozone trends over southern China, Atmos. Environ., 220, 117060, https://doi.org/10.1016/j.atmosenv.2019.117060, 2020.

Cirelli, D., Equiza, M. A., Lieffers, V. J., and Tyree, M. T.: *Populus* species from diverse habitats maintain high night-time conductance under drought, Tree Physiol., 36, 229-242, https://doi.org/10.1093/treephys/tpv092, 2016.

Dias-Junior, C. Q., Dias, N. L., Fuentes, J. D., and Chamecki, M.: Convective storms and non-classical low-level jets during high ozone level episodes in the Amazon region: An ARM/GOAMAZON case study, Atmos. Environ., 155, 199-209, https://doi.org/10.1016/j.atmosenv.2017.02.006, 2017.

Du, Y. and Chen, G.: Heavy rainfall associated with double low-level jets over southern China. Part II: Convection initiation, Mon. Weather Rev., 147, 543-565, https://doi.org/10.1175/mwr-d-18-0102.1, 2019.

Emmons, L. K., Walters, S., Hess, P. G., Lamarque, J. F., Pfister, G. G., Fillmore, D., Granier, C., Guenther, A., Kinnison, D., Laepple, T., Orlando, J., Tie, X., Tyndall, G., Wiedinmyer, C., Baughcum, S. L., and Kloster, S.: Description and evaluation of the Model for Ozone and Related chemical Tracers, version 4 (MOZART-4), Geosci. Model. Dev., 3, 43-67, https://doi.org/10.5194/gmd-3-43-2010, 2010.

https://doi.org/10.5194/acp-2022-360
Preprint. Discussion started: 14 June 2022


Atmospheric Chemistry and Physics Discussions

EPA.: Guidance on the use of models and other analyses for demonstrating attainment of air quality goals for ozone, PM2.5, and regional haze. https://www.epa.gov/sites/default/files/2020-10/documents/final-03-pm-rh-guidance.pdf, 2017.

George, J. J.: Weather forecasting for aeronautics. Academic press, https://doi.org/10.1016/C2013-0-12567-6, 1960.

Gong, D., Wang, H., Zhang, S., Wang, Y., Liu, S. C., Guo, H., Shao, M., He, C., Chen, D., He, L., Zhou, L., Morawska, L., Zhang, Y., and Wang, B.: Low-level summertime isoprene observed at a forested mountaintop site in southern China: Implications for strong regional atmospheric oxidative capacity, Atmos. Chem. Phys., 18, 14417-14432, https://doi.org/10.5194/acp-18-14417-2018, 2018.

Grant, D. D., Fuentes, J. D., DeLonge, M. S., Chan, S., Joseph, E., Kucera, P., Ndiaye, S. A., and Gaye, A. T.: Ozone transport by mesoscale convective storms in western Senegal, Atmos. Environ., 42, 7104-7114, https://doi.org/10.1016/j.atmosenv.2008.05.044, 2008.

Grell, G. A. and Dévényi, D.: A generalized approach to parameterizing convection combining ensemble and data assimilation techniques, Geophys. Res. Lett., 29, 381-384, https://doi.org/10.1029/2002gl015311, 2002.

Guenther, A., Karl, T., Harley, P., Wiedinmyer, C., Palmer, P. I., and Geron, C.: Estimates of global terrestrial isoprene emissions using MEGAN (Model of Emissions of Gases and Aerosols from Nature), Atmos. Chem. Phys., 6, 3181-3210, https://doi.org/10.5194/acp-6-3181-2006, 2006.

Han, C., Liu, R., Luo, H., Li, G., Ma, S., Chen, J., and An, T.: Pollution profiles of volatile organic compounds from different urban functional areas in Guangzhou China based on GC/MS and PTR-TOF-MS: Atmospheric environmental implications, Atmos. Environ., 214, 116843, https://doi.org/10.1016/j.atmosenv.2019.116843, 2019.

He, Y., Wang, H., Wang, H., Xu, X., Li, Y., and Fan, S.: Meteorology and topographic influences on nocturnal ozone increase during the summertime over Shaoguan, China, Atmos. Environ., 256, 118459, https://doi.org/10.1016/j.atmosenv.2021.118459, 2021.

Hersbach, H., Bell, B., Berrisford, P., Hirahara, S., Horányi, A., Muñoz-Sabater, J., Nicolas, J., Peubey, C., Radu, R., Schepers, D., Simmons, A., Soci, C., Abdalla, S., Abellan, X., Balsamo, G., Bechtold, P., Biavati, G., Bidlot, J., Bonavita, M., Chiara, G., Dahlgren, P., Dee, D., Diamantakis, M., Dragani, R., Flemming, J., Forbes, R., Fuentes, M., Geer, A., Haimberger, L., Healy, S., Hogan, R. J., Hólm, E., Janisková, M., Keeley, S., Laloyaux, P., Lopez, P., Lupu, C., Radnoti, G., Rosnay, P., Rozum, I., Vamborg, F., Villaume, S., and Thépaut, J. N.: The ERA5 global reanalysis, Q. J. R. Meteorol. Soc., 146, 1999-2049, https://doi.org/10.1002/qj.3803, 2020.

HKEPD.: Pearl River Delta Regional Air Quality Monitoring Report for Year 2017. https://www.epd.gov.hk/epd/sites/default/files/epd/english/resources_pub/publications/files/PRD_2017_report_en.pdf, 2017.

Hodges, D. and Pu, Z. X.: Characteristics and variations of low-level jets and environmental factors associated with summer precipitation extremes over the Great Plains, J. Clim., 32, 5123-5144, https://doi.org/10.1175/jcli-d-18-0553.1, 2019.

Hu, X. M., Klein, P. M., Xue, M., Zhang, F., Doughty, D. C., Forkel, R., Joseph, E., and Fuentes, J. D.: Impact of the vertical mixing induced by low-level jets on boundary layer ozone concentration, Atmos. Environ., 70, 123-130, https://doi.org/10.1016/j.atmosenv.2012.12.046, 2013.

Iacono, M. J., Delamere, J. S., Mlawer, E. J., Shephard, M. W., Clough, S. A., and Collins, W. D.: Radiative forcing by long-lived greenhouse gases: Calculations with the AER radiative transfer models, J. Geophys. Res. Atmos., 113, https://doi.org/10.1029/2008jd009944, 2008.

Jacob, D. J.: Heterogeneous chemistry and tropospheric ozone, Atmos. Environ., 34, 2131-2159, https://doi.org/10.1016/S1352-2310(99)00462-8, 2000.

Jain, S. L., Arya, B. C., Kumar, A., Ghude, S. D., and Kulkarni, P. S.: Observational study of surface ozone at New Delhi, India, Int. J. Remote Sens., 26, 3515-3524, https://doi.org/10.1080/01431160500076616, 2007.

Jiménez, P., Parra, R., and Baldasano, J. M.: Influence of initial and boundary conditions for ozone modeling in very complex terrains: A case study in the northeastern Iberian Peninsula, Environ. Model. Softw., 22, 1294-1306, https://doi.org/10.1016/j.envsoft.2006.08.004, 2007.

Johnson, D. L.: A stability analysis of AVE-IV severe weather sounding, NASA Tech. Paper, 2045-2126, 1982.

Klein, A., Ravetta, F., Thomas, J. L., Ancellet, G., Augustin, P., Wilson, R., Dieudonné, E., Fourmentin, M., Delbarre, H., and Pelon, J.: Influence of vertical mixing and nighttime transport on surface ozone variability in the morning in Paris and the surrounding region, Atmos. Environ., 197, 92-102, https://doi.org/10.1016/j.atmosenv.2018.10.009, 2019.

https://doi.org/10.5194/acp-2022-360
Preprint. Discussion started: 14 June 2022

Atmospheric Chemistry and Physics Discussions
Open Access
EGU

Kleinman, L., Lee, Y. N., Springston, S. R., Nunnermacker, L., Zhou, X., Brown, R., Hallock, K., Klotz, P., Leahy, D., and Lee, J. H.: Ozone formation at a rural site in the southeastern United States, J. Geophys. Res. Atmos., 99, 3469-3482, https://doi.org/10.1029/93JD02991, 1994.

Kuang, S., Newchurch, M. J., Burris, J., Wang, L., Buckley, P. I., Johnson, S., Knupp, K., Huang, G., Phillips, D., and Cantrell, W.: Nocturnal ozone enhancement in the lower troposphere observed by lidar, Atmos. Environ., 45, 6078-6084, https://doi.org/10.1016/j.atmosenv.2011.07.038, 2011.

Kulkarni, P. S., Bortoli, D., and Silva, A. M.: Nocturnal surface ozone enhancement and trend over urban and suburban sites in Portugal, Atmos. Environ., 71, 251-259, https://doi.org/10.1016/j.atmosenv.2013.01.051, 2013.

Kulkarni, P. S., Bortoli, D., Silva, A. M., and Reeves, C. E.: Enhancements in nocturnal surface ozone at urban sites in the UK, Environ. Sci. Pollut. Res., 22, 20295-20305, https://doi.org/10.1007/s11356-015-5259-z, 2015.

Kurt, O. K., Zhang, J., and Pinkerton, K. E.: Pulmonary health effects of air pollution, Curr. Opin. Pulm. Med., 22, 138-143, https://doi.org/10.1097/MCP.0000000000000248, 2016.

Li, X. B., Yuan, B., Parrish, D. D., Chen, D., Song, Y., Yang, S., Liu, Z., and Shao, M.: Long-term trend of ozone in southern China reveals future mitigation strategy for air pollution, Atmos. Environ., 269, 118869, https://doi.org/10.1016/j.atmosenv.2021.118869, 2022.

Li, Y., Wang, W., Chang, M., and Wang, X.: Impacts of urbanization on extreme precipitation in the Guangdong-Hong Kong-Macau Greater Bay Area, Urban Clim., 38, 100904, https://doi.org/10.1016/j.uclim.2021.100904, 2021.

Liao, Z., Ling, Z., Gao, M., Sun, J., Zhao, W., Ma, P., Quan, J., and Fan, S.: Tropospheric ozone variability over Hong Kong based on recent 20 years (2000–2019) ozonesonde observation, J. Geophys. Res. Atmos., 126, e2020JD033054, https://doi.org/10.1029/2020jd033054, 2021.

Lin, Y., Farley, R. D., and Orville, H. D.: Bulk parameterization of the snow field in a cloud model, J. Appl. Meteorol. Climatol., 22, 1065-1092, https://doi.org/10.1175/1520-0450(1983)022<1065:BPOTSF>2.0.CO;2, 1983.

Liu, H., Zhang, M., and Han, X.: A review of surface ozone source apportionment in China, Atmos. Ocean. Sci. Lett., 13, 470-484, https://doi.org/10.1080/16742834.2020.1768025, 2020.

Liu, X. H., Zhang, Y., Xing, J., Zhang, Q., Wang, K., Streets, D. G., Jang, C., Wang, W., and Hao, J. M.: Understanding of regional air pollution over China using CMAQ, part II. Process analysis and sensitivity

https://doi.org/10.5194/acp-2022-360
Preprint. Discussion started: 14 June 2022

Atmospheric Chemistry and Physics Discussions

of ozone and particulate matter to precursor emissions, Atmos. Environ., 44, 3719-3727, https://doi.org/10.1016/j.atmosenv.2010.03.036, 2010.

Lu, K., Zhang, Y., Su, H., Shao, M., Zeng, L., Zhong, L., Xiang, Y., Chang, C., Chou, C. K. C., and Wahner, A.: Regional ozone pollution and key controlling factors of photochemical ozone production in Pearl River Delta during summer time, Sci. China Chem., 53, 651-663, https://doi.org/10.1007/s11426-010-0055-6, 2010.

Ma, Z., Xu, J., Quan, W., Zhang, Z., Lin, W., and Xu, X.: Significant increase of surface ozone at a rural site, north of eastern China, Atmos. Chem. Phys., 16, 3969-3977, https://doi.org/10.5194/acp-16-3969-2016, 2016.

Mao, J., Yan, F., Zheng, L., You, Y., Wang, W., Jia, S., Liao, W., Wang, X., and Chen, W.: Ozone control strategies for local formation- and regional transport-dominant scenarios in a manufacturing city in southern China, Sci. Total Environ., 813, 151883, https://doi.org/10.1016/j.scitotenv.2021.151883, 2022.

Marelle, L., Myhre, G., Steensen, B. M., Hodnebrog, Ø., Alterskjær, K., and Sillmann, J.: Urbanization in megacities increases the frequency of extreme precipitation events far more than their intensity, Environ. Res. Lett., 15, 124072, https://doi.org/10.1088/1748-9326/abcc8f, 2020.

Monin, A. S. and Obukhov, A. M.: Basic laws of turbulent mixing in the surface layer of the atmosphere, Contrib. Geophys. Inst. Acad. Sci. USSR, 151, e187, https://gibbs.science/efd/handouts/monin_obukhov_1954.pdf, 1954.

MEP.: The ministry of environmental protection of China. Guidelines for selection of ambient air quality models (Trial). https://english.mee.gov.cn/Resources/standards/Air_Environment/quality_standard1/201605/t20160511_337502.shtml, 2015.

Nair, P. R., Chand, D., Lal, S., Modh, K. S., Naja, M., Parameswaran, K., Ravindran, S., and Venkataramani, S.: Temporal variations in surface ozone at Thumba (8.6 °N, 77 °E) - a tropical coastal site in India, Atmos. Environ., 36, 603-610, https://doi.org/10.1016/S1352-2310(01)00527-1, 2002.

Nakanishi, M. and Niino, H.: An improved Mellor–Yamada Level-3 model: Its numerical stability and application to a regional prediction of advection fog, Boundary-Layer Meteorol., 119, 397-407, https://doi.org/10.1007/s10546-005-9030-8, 2006.

Olauson, J.: ERA5: The new champion of wind power modelling?, Renew. Energ., 126, 322-331, https://doi.org/10.1016/j.renene.2018.03.056, 2018.

Prtenjak, M. T., Jeričević, A., Klaić, Z. B., Alebić-Juretić, A., and Bulić, I. H.: Atmospheric dynamics and elevated ozone concentrations in the northern Adriatic, Meteorol. Appl., 20, 482-496, https://doi.org/10.1002/met.1312, 2013.

Ravishankara, A. R.: Are chlorine atoms significant tropospheric free radicals?, Proc. Natl. Acad. Sci. U. S. A., 106, 13639-13640, https://doi.org/10.1073/pnas.0907089106, 2009.

Salmond, J. A. and McKendry, I. G.: Secondary ozone maxima in a very stable nocturnal boundary layer: Observations from the Lower Fraser Valley, BC, Atmos. Environ., 36, 5771-5782, https://doi.org/10.1016/S1352-2310(02)00698-2, 2002.

Seibert, P., Feldmann, H., Neininger, B., Baumle, M., and Trickl, T.: South foehn and ozone in the Eastern Alps - case study and climatological aspects, Atmos. Environ., 34, 1379-1394, https://doi.org/10.1016/S1352-2310(99)00439-2, 2000.

Seto, K. C., Guneralp, B., and Hutyra, L. R.: Global forecasts of urban expansion to 2030 and direct impacts on biodiversity and carbon pools, Proc. Natl. Acad. Sci. U. S. A., 109, 16083-16088, https://doi.org/10.1073/pnas.1211658109, 2012.

Shen, J., Zhang, Y., Wang, X., Li, J., Chen, H., Liu, R., Zhong, L., Jiang, M., Yue, D., Chen, D., and Lv, W.: An ozone episode over the Pearl River Delta in October 2008, Atmos. Environ., 122, 852-863, https://doi.org/10.1016/j.atmosenv.2015.03.036, 2015.

Shith, S., Awang, N. R., Latif, M. T., and Ramli, N. A.: Fluctuations in nighttime ground-level ozone concentrations during haze events in Malaysia, Air Qual. Atmos. Hlth., 14, 19-26, https://doi.org/10.1007/s11869-020-00908-5, 2021.

Sousa, S. I. V., Alvim-Ferraz, M. C. M., and Martins, F. G.: Identification and origin of nocturnal ozone maxima at urban and rural areas of northern Portugal – Influence of horizontal transport, Atmos. Environ., 45, 942-956, https://doi.org/10.1016/j.atmosenv.2010.11.008, 2011.

Stull, R. B.: An introduction to boundary layer meteorology, Springer Science & Business Media, 1988.

Sullivan, J. T., Rabenhorst, S. D., Dreessen, J., McGee, T. J., Delgado, R., Twigg, L., and Sumnicht, G.: Lidar observations revealing transport of O3 in the presence of a nocturnal low-level jet: Regional implications for "next-day" pollution, Atmos. Environ., 158, 160-171, https://doi.org/10.1016/j.atmosenv.2017.03.039, 2017.

Tong, N. Y. O. and Leung, D. Y. C.: Ozone diurnal characteristics in areas with different urbanisations, Int. J. Environ. Pollut., 49, 100-124, https://doi.org/10.1504/Ijep.2012.049771, 2012.

Trier, S. B., Wilson, J. W., Ahijevych, D. A., and Sobash, R. A.: Mesoscale vertical motions near nocturnal convection initiation in PECAN, Mon. Weather Rev., 145, 2919-2941, https://doi.org/10.1175/mwr-d-17-0005.1, 2017.

Udina, M., Soler, M. R., Olid, M., Jiménez-Esteve, B., and Bech, J.: Pollutant vertical mixing in the nocturnal boundary layer enhanced by density currents and low-level jets: Two representative case studies, Boundary-Layer Meteorol., 174, 203-230, https://doi.org/10.1007/s10546-019-00483-y, 2019.

Wang, T., Xue, L., Brimblecombe, P., Lam, Y. F., Li, L., and Zhang, L.: Ozone pollution in China: A review of concentrations, meteorological influences, chemical precursors, and effects, Sci. Total. Environ., 575, 1582-1596, https://doi.org/10.1016/j.scitotenv.2016.10.081, 2017.

Wang, T., Wei, X. L., Ding, A. J., Poon, C. N., Lam, K. S., Li, Y. S., Chan, L. Y., and Anson, M.: Increasing surface ozone concentrations in the background atmosphere of southern China, 1994-2007, Atmos. Chem. Phys., 9, 6217-6227, https://doi.org/10.5194/acp-9-6217-2009, 2009.

Wang, X., Situ, S., Guenther, A., Chen, F. E. I., Wu, Z., Xia, B., and Wang, T.: Spatiotemporal variability of biogenic terpenoid emissions in Pearl River Delta, China, with high-resolution land-cover and meteorological data, Tellus B Chem. Phys. Meteorol., 63, 241-254, https://doi.org/10.1111/j.1600-0889.2010.00523.x, 2011.

Wang, X., Zhang, Y., Hu, Y., Zhou, W., Lu, K., Zhong, L., Zeng, L., Shao, M., Hu, M., and Russell, A. G.: Process analysis and sensitivity study of regional ozone formation over the Pearl River Delta, China, during the PRIDE-PRD2004 campaign using the Community Multiscale Air Quality modeling system, Atmos. Chem. Phys., 10, 4423-4437, https://doi.org/10.5194/acp-10-4423-2010, 2010.

Wyat Appel, K., Napelenok, S., Hogrefe, C., Pouliot, G., Foley, K. M., Roselle, S. J., Pleim, J. E., Bash, J., Pye, H. O. T., Heath, N., Murphy, B., and Mathur, R.: Overview and evaluation of the Community Multiscale Air Quality (CMAQ) modeling system version 5.2, in: Air Pollution Modeling and its Application XXV, Springer Proceedings in Complexity, 69-73, https://doi.org/10.1007/978-3-319-57645-9_11, 2018.

Xue, L., Wang, T., Louie, P. K., Luk, C. W., Blake, D. R., and Xu, Z.: Increasing external effects negate local efforts to control ozone air pollution: A case study of Hong Kong and implications for other Chinese cities, Environ. Sci. Technol., 48, 10769-10775, https://doi.org/10.1021/es503278g, 2014.

Yang, C., Li, Q., Hu, Z., Chen, J., Shi, T., Ding, K., and Wu, G.: Spatiotemporal evolution of urban agglomerations in four major bay areas of US, China and Japan from 1987 to 2017: Evidence from remote sensing images, Sci. Total. Environ., 671, 232-247, https://doi.org/10.1016/j.scitotenv.2019.03.154, 2019a.

Yang, L., Luo, H., Yuan, Z., Zheng, J., Huang, Z., Li, C., Lin, X., Louie, P. K. K., Chen, D., and Bian, Y.: Quantitative impacts of meteorology and precursor emission changes on the long-term trend of ambient ozone over the Pearl River Delta, China, and implications for ozone control strategy, Atmos. Chem. Phys., 19, 12901-12916, https://doi.org/10.5194/acp-19-12901-2019, 2019b.

Yue, X., Unger, N., Harper, K., Xia, X., Liao, H., Zhu, T., Xiao, J., Feng, Z., and Li, J.: Ozone and haze pollution weakens net primary productivity in China, Atmos. Chem. Phys., 17, 6073-6089, https://doi.org/10.5194/acp-17-6073-2017, 2017.

Yusoff, M. F., Latif, M. T., Juneng, L., Khan, M. F., Ahamad, F., Chung, J. X., and Mohtar, A. A. A.: Spatio-temporal assessment of nocturnal surface ozone in Malaysia, Atmos. Environ., 207, 105-116, https://doi.org/10.1016/j.atmosenv.2019.03.023, 2019.

Zhang, B., Li, J., Wang, M., Duan, P., and Li, C.: Using DMSP/OLS and NPP/VIIRS images to analyze the expansion of 21 urban agglomerations in mainland China, J. Urban Plan. Dev., 147, 04021024, https://doi.org/10.1061/(asce)up.1943-5444.0000690, 2021.

Zhang, R., Lei, W., Tie, X., and Hess, P.: Industrial emissions cause extreme urban ozone diurnal variability, Proc. Natl. Acad. Sci. U. S. A., 101, 6346-6350, https://doi.org/10.1073/pnas.0401484101, 2004.

Zheng, B., Tong, D., Li, M., Liu, F., Hong, C., Geng, G., Li, H., Li, X., Peng, L., Qi, J., Yan, L., Zhang, Y., Zhao, H., Zheng, Y., He, K., and Zhang, Q.: Trends in China's anthropogenic emissions since 2010 as the consequence of clean air actions, Atmos. Chem. Phys., 18, 14095-14111, https://doi.org/10.5194/acp-18-14095-2018, 2018.

Zhong, Z., Zheng, J., Zhu, M., Huang, Z., Zhang, Z., Jia, G., Wang, X., Bian, Y., Wang, Y., and Li, N.: Recent developments of anthropogenic air pollutant emission inventories in Guangdong province, China, Sci. Total Environ., 627, 1080-1092, https://doi.org/10.1016/j.scitotenv.2018.01.268, 2018.

Zhu, X. W., Ma, Z. Q., Li, Z. M., Wu, J., Guo, H., Yin, X. M., Ma, X. H., and Qiao, L.: Impacts of meteorological conditions on nocturnal surface ozone enhancement during the summertime in Beijing, Atmos. Environ., 225, 117368, https://doi.org/10.1016/j.atmosenv.2020.117368, 2020.